A 3D analysis of yeast ER structure reveals how ER domains are organized by membrane curvature

Matt West,[1] Nesia Zurek,[1] Andreas Hoenger,[1,2] and Gia K. Voeltz[1]

[1]Department of Molecular, Cellular, and Developmental Biology, University of Colorado, Boulder, CO 80309
[2]Boulder Laboratory for 3D Electron Microscopy of Cells, Boulder, CO 80309

We analyzed the structure of yeast endoplasmic reticulum (ER) during six sequential stages of budding by electron tomography to reveal a three-dimensional portrait of ER organization during inheritance at a nanometer resolution. We have determined the distribution, dimensions, and ribosome densities of structurally distinct but continuous ER domains during multiple stages of budding with and without the tubule-shaping proteins, reticulons (Rtns) and Yop1. In wild-type cells, the peripheral ER contains cytoplasmic cisternae, many tubules, and a large plasma membrane (PM)–associated ER domain that consists of both tubules and fenestrated cisternae. In the absence of Rtn/Yop1, all three domains lose membrane curvature, ER ribosome density changes, and the amount of PM-associated ER increases dramatically. Deletion of Rtns/Yop1 does not, however, prevent bloated ER tubules from being pulled from the mother cisterna into the bud and strongly suggests that Rtns/Yop1 stabilize/maintain rather than generate membrane curvature at all peripheral ER domains in yeast.

Introduction

In all eukaryotes, the peripheral ER branches out of the nuclear envelope (NE) as a membrane network of interconnected tubules and cisternae with a single lumen (Estrada de Martin et al., 2005a; English et al., 2009). The ER has an elaborate and conserved shape, and yet, little is known about how ER domains are shaped and distributed by membrane proteins. The ER domains that are most obvious by fluorescence microscopy are peripheral ER cisternae and tubules. The cisternal regions consist of relatively flat parallel membrane bilayers separated by a lumen and have low membrane curvature. The cisternae are interconnected with the rest of the ER network, which can be mostly tubular in shape. In contrast to cisternae, tubules have high membrane curvature in cross section with reported diameters of <100 nm (Staehelin, 1997; Prinz et al., 2000; Hu et al., 2008).

Two protein families, the reticulons (Rtns) and DP1/Yop1, have been shown to shape the membrane bilayer of ER tubules in multiple eukaryotes, including animals, plants, and yeast (De Craene et al., 2006; Voeltz et al., 2006; Audhya et al., 2007; Anderson and Hetzer, 2008; Tolley et al., 2008). They partition within the ER to the ER tubules and do not localize to the flat membranes of the NE or peripheral ER cisternae (Voeltz et al., 2006). Rtn overexpression in yeast and animal cells generates longer unbranched tubules and fewer cisternae, whereas depletion propagates cisternae at the expense of tubular ER (tubER; Voeltz et al., 2006; Anderson and Hetzer, 2008). Furthermore, reconstitution of Rtn/Yop1 proteins into proteoliposomes can result in the formation of membrane tubules (Hu et al., 2008).

The cytoskeleton also functions to shape the ER membrane (English et al., 2009). In animal cells, ER tubules are pulled out of ER membranes by motor proteins moving along microtubules (MTs; Lee and Chen, 1988; Waterman-Storer and Salmon, 1998; Grigoriev et al., 2008; Woźniak et al., 2009; Friedman et al., 2010). Depolymerization of MTs causes the ER to retract, and tubules collapse into cisternae despite the presence of endogenous Rtns (Terasaki et al., 1986; Lu et al., 2009). By overexpressing an Rtn protein, Rtn4a, the tubules persist for longer in the absence of MTs (Shibata et al., 2008). However, these data do argue that endogenous levels of these membrane-shaping proteins cannot overcome the effects of depleting MTs in the cell. During mitosis in animal cells, the shape of the ER becomes almost entirely cisternal, and it has been proposed that this mitotic change in ER shape could also be caused by the

Correspondence to Gia K. Voeltz: gia.voeltz@colorado.edu

Abbreviations used in this paper: cecER, central cisternal ER; FS, freeze substituted; HPF, high-pressure frozen; MT, microtubule; NE, nuclear envelope; ONM, outer nuclear membrane; PM, plasma membrane; pmaER, PM-associated ER; Rtn, reticulon; TEM, transmission EM; tubER, tubular ER; wt, wild type.

Supplemental material can be found at:
http://doi.org/10.1083/jcb.201011039

The Rockefeller University Press $30.00
J. Cell Biol. Vol. 193 No. 2 333–346
www.jcb.org/cgi/doi/10.1083/jcb.201011039

dramatic reorganization of the MT cytoskeleton (Lu et al., 2009). MTs are not required for peripheral ER structure in yeast (Du et al., 2004). In yeast, the actin cytoskeleton is also dispensable once cortical ER structure has formed. However, actin is required during the inheritance of peripheral ER into the growing bud (Prinz et al., 2000; Estrada et al., 2003; Du et al., 2004).

Very little is known about how cisternae are shaped. Two predominant hypotheses exist for what determines the amount of tubules and cisternae: (1) the first is that it depends on the abundance of Rtn proteins that would favor tubules over cisternae; (2) in addition, it has been proposed that cisternae might be generated and stabilized by polyribosomes binding and flattening the ER membrane (Shibata et al., 2006, 2010; Puhka et al., 2007). Historically, cisternae are considered polyribosome-bound "rough" ER, and tubules are referred to as "smooth" ER devoid of bound ribosomes. This is because EM shows secretory cells with massive cisternae that are studded with ribosomes, and these images have been compared with those of muscle cells that have an entirely tubER devoid of ribosomes (Shibata et al., 2006). However, ER ribosome density has never been compared directly in cell types that contain multiple ER domains, such as the asymmetric budding yeast. A thorough ribosome map would demonstrate whether ribosome density on the ER is correlated at all with ER membrane shape. Recently, Rtn proteins were also shown to partition preferentially into the edges of cisternae, suggesting that they may also contribute to the shape of this region of membrane curvature (Kiseleva et al., 2007; Schuck et al., 2009; Shibata et al., 2010; Sparkes et al., 2010).

The yeast *Saccharomyces cerevisiae* is one of the most revealing model organisms for studying various ER functions. Our goal was to visualize the organization of yeast ER domains at high resolution in the absence and presence of the tubule-shaping proteins Rtns and Yop1 to gain insight into their role in generating and/or maintaining ER shape and distribution. We have analyzed ER structure by serial section transmission EM (TEM) and serial semithick section (150–200 nm) dual-axis electron tomography of high-pressure frozen (HPF) and rapid freezing–freeze substituted (FS) fixation of yeast cells solved with the software package IMOD (Kremer et al., 1996). We have mapped the 3D structure of the ER within six different yeast cells with different bud sizes at a nanometer resolution. These data have allowed us to characterize (a) the spatial organization of yeast ER domains within the cytoplasm, (b) the extent of contact between the ER and the plasma membrane (PM), (c) the dimensions of all ER domains, including cisternae, tubules, and PM-associated ER (pmaER), (d) the relationship between membrane curvature and ribosome density, and (e) ER structure during inheritance into the growing bud. We then compared these 3D structures to the ER structure in yeast lacking the tubule-shaping proteins Rtns (Rtn1 and Rtn2) and Yop1. We determined that Rtns/Yop1 contribute to the membrane curvature, distribution, dimensions, and ribosome density of all ER domains. Furthermore, our data suggest a role for these Rtns/Yop1 in stabilizing/maintaining rather than generating membrane curvature in yeast.

Results

A detailed 3D EM structure reveals the domain organization of yeast peripheral ER

We imaged the yeast ER by TEM and dual-axis electron tomography to visualize its 3D structure. Haploid cells of budding yeast were grown to log phase, HPF, and FS in a manner that optimizes membrane contrast with minimal stain and fixation artifacts (see Materials and methods; described in Nickerson et al., 2010). Well-fixed samples within bud diameter constraints and uniformly labeled by fiducial gold were chosen for tomography. The first cell we analyzed was mitotic with a bud diameter of 665 nm. The bud sizes reflect the diameter of a circle that fits from the tip to the base of the bud (Fig. S1). Four serial 200-nm sections were combined to cover a cellular volume of 0.92 μm^3 with some sample loss caused by microtomy ($\sim$20 nm of the z axis) between serial sections. All membrane structures within the combined sections were manually assigned at 5-nm intervals using IMOD software (Kremer et al., 1996; Murk et al., 2003; Höög et al., 2007). After tomographic reconstruction, the ER was identified because (a) it was ribosome bound and (b) all domains were continuous with each other and shared a membrane bilayer that could be connected back to the NE. Golgi, mitochondria, vacuoles, and vesicles were also identified based on the similarity between their 3D structures and those reported in the literature (O'Toole et al., 2002; Marsh et al., 2004). The reconstruction reveals the 3D structure of all ER domains within this volume at about the resolution of the membrane bilayer ($\sim$4 nm, Crowther relation; Koster et al., 1997). The four main ER domains are depicted in our tomogram (Fig. 1, A–E, the NE [orange], central cisternal ER [cecER], tubER, and pmaER).

The 3D EM reconstruction of this cell reveals new information about the ER structure in yeast (Fig. 1 B). For example, two types of peripheral ER domains can be found branching out of the outer nuclear membrane (ONM) with a lumen that is continuous with that of the NE: cecER and tubER (Fig. 1, C and D, respectively). Previous studies refer to the ER regions that traverse the cytoplasm of yeast cells as tubular (Preuss et al., 1991; Achleitner et al., 1999; Prinz et al., 2000). We typically find six to eight tubules branching out of the NE (one example in Fig. 1 D). However, we also observe a single cecER traversing from the NE through the cytoplasm (Fig. 1, A–C, yellow domain). The cecER has not been described before even though it makes up a significant amount of ER volume. By 2D TEM, it resembles a tubule, but the 3D structure reveals that this domain is in fact a massive cisterna (Fig. 1 B). In this cell, the cecER points from the NE toward the bud. The cecER has three defining features: (1) it is more ribosome dense than the tubules connected to the NE (Fig. 1 C, ribosomes are black dots, and the bound example is marked with a red arrow), (2) it can usually be traced all the way from the ONM to the cortical ER, and (3) the contact it makes with the NE in all of our examples triangulates at the base as it meets the ONM, whereas the tubules constrict (Fig. 1, C and D, compare ONM contact). tubER is found throughout the cytoplasm. It forms connections between the NE and the cecER, between the cecER and the pmaER, and between pmaER domains (Fig. 1, A and D). tubER is also seen forming contacts with other organelles.

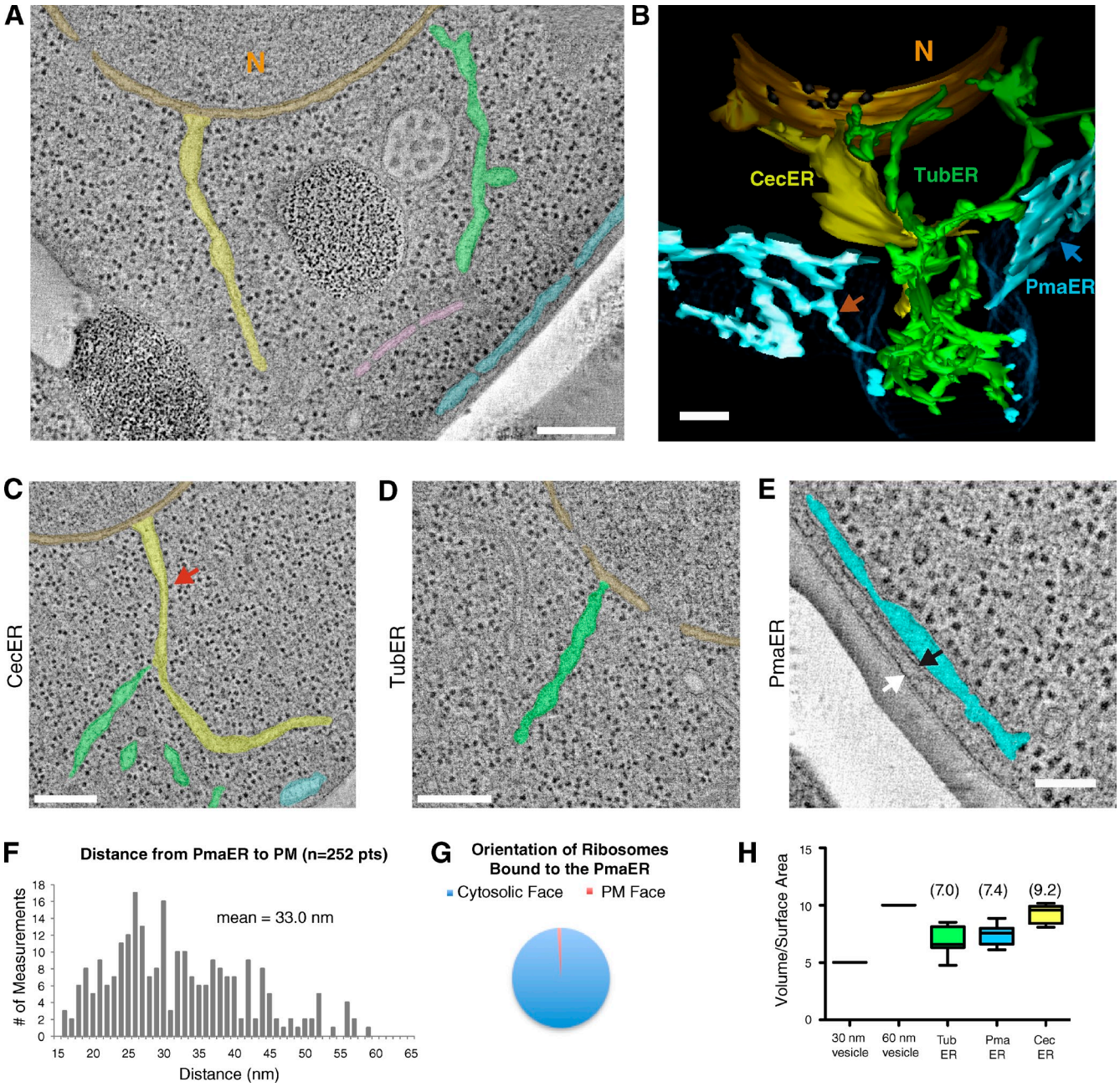

Figure 1. **3D structural analysis of ER morphology.** (A and B) 2D tomograph derived from a 200-nm-thick section shows the NE (orange), pmaER, cecER, tubER, and Golgi (pink; A) and corresponding 3D model (of A) shows all ER domains in a wt yeast cell (bud size = 665 nm; B). The blue shade is the PM. N is the nucleus. Black holes on the NE are nuclear pores. The orange arrow points to a more tubular pmaER structure, whereas the blue arrow points to a fenestrated cisternal pmaER. (C–E) 2D tomograph of cecER (C), tubER (D), and pmaER (with white and black arrows pointing at PM and ER membranes, respectively; E). Note that the black dots are ribosomes (red arrow in C). (F) Range of measured distances between the pmaER and PM membranes (e.g., from black to white arrows in E). (G) The percentage of ribosomes bound to the cytosolic versus PM face of the pmaER demonstrates that the PM face is mostly ribosome excluded. (H) Volume/surface area ratios were calculated from our 3D models for vesicles (30 and 60 nm), tubER, pmaER, and cecER. Brackets show range of measurements, and boxes show SEM. Horizontal lines show means given above the boxes. Bars: (A, C, and D) 200 nm; (B) 100 nm; (E) 50 nm.

pmaER is a unique ER domain

The pmaER has previously been referred to as cortical ER and was described as a tubular network that underlies the PM (Preuss et al., 1991; Prinz et al., 2000; Voeltz et al., 2002). However, the 3D structure reveals that the pmaER has regions that are tubular (Fig. 1 B, orange arrow) and other regions that are cisternal and highly fenestrated (Fig. 1 B, blue arrow). Recent work shows hints of the fenestrated structure even by fluorescence microscopy (Schuck et al., 2009). Several properties define the pmaER as a distinct ER domain. The most obvious is that the pmaER is closely apposed to the PM (Pichler et al., 2001). To determine the distance between the cytoplasmic surface of the PM to the surface of the pmaER (Fig. 1 E, distance between arrow tips), we chose ideal 3D peripheral regions and measured the spacing at 50-nm intervals. We obtained 252 distance measurements over a total surface area of 0.63 μm^2, which were

graphed in a histogram and revealed a range from 15.7 to 58.9 with a mean spacing of 33.0 nm (Fig. 1 F). These two membranes are so closely apposed over such a large area that ribosomes are >99% excluded from the PM face of the pmaER (Fig. 1, E [image] and G [graph]).

cecER, tubER, and pmaER have different ER lumenal volume to surface area ratio

We used our 3D models to calculate the lumenal volume to surface area (V/SA) ratios of all three ER domains. We measured the volume to surface area ratios for several regions in our models that were unambiguously tubER, cecER, and pmaER (Fig. 1 H, mean V/SA_{tubER} = 7.0, V/SA_{cecER} = 9.2, and V/SA_{pmaER} = 7.4). We also calculated for comparison the volume to surface area ratios of 30- and 60-nm vesicles present in our samples (V/SA = 5.0 and 10.0, respectively). These data reveal that ER domain shape affects the lumenal volume to membrane surface area ratios. In yeast, the cecER has a larger volume to surface area ratio than tubER and pmaER, which suggests that tubER could be better suited for functions that require a lot of membrane surface area, whereas cecER may be adapted for lumenal processes.

ER domain abundance and organization in the mother cell during inheritance

To determine ER domain distribution during inheritance, we compared the organization of wild-type (wt) yeast ER during a total of six different budding stages. For each cell, three to four 200-nm-thick sections were reconstructed into serial tomograms. We aligned the images so that the viewpoint is approximately perpendicular to the mother–bud axis, and the cells were ordered according to bud size (bud A = 371 nm, B = 383 nm, C = 665 nm, D = 908 nm, E = 1,095 nm, and F = 1,255 nm). Tomographs for each cell analyzed are shown (Fig. S2, A–F, left). We mapped the structure of all three peripheral ER domains in all six mother cells (Fig. 2, A–F, left). ER domains are color coded as in Fig. 1 (Fig 2, A–F, the position of the PM is shown as a fine blue mesh). The pmaER (regardless of whether it is cisternal or tubular in shape) was assigned based solely on its position relative to the PM, whereas cytoplasmic tubER and cecER domains were assigned based on their 3D structures. In regions where the tubER and cecER domains were either structurally ambiguous or in transition, they were colored as either tubER or cecER depending on their volume to surface area ratios (Fig. 1 H). We also traced Golgi and vesicles present in our tomograms, which could be discriminated from the ER domains (Fig. S2, A–F, right). Some of these cytoplasmic vesicles are very close to the ER membrane and could be either COPII vesicles leaving or COPI vesicles returning to the ER (Fig. S3, blue vesicles are within 10 nm of the ER membrane, and purple vesicles are farther away). We have included videos to show tomographic sections and 3D rotating models of organelle structures within each of the six cells (Videos 1, 2, 3, 4, 5, and 6; corresponding to cells in Fig 2, A–F).

We calculated the volume and relative abundance of each peripheral ER domain present in our reconstructions for each of the mother and daughter cells. The measured volume and percentage of each ER domain in the mother is shown in Fig. 2 (G and H). Each of the three ER domains (pmaER, tubER, and cecER) represents roughly a third of the ER present in the mother during the first five stages. The cecER constitutes a major ER domain in the mother for the cells with the five smallest buds (Fig. 2, A–E). Interestingly, the leading edge of the cecER points roughly toward the bud in all five. This orientation suggests that cecER could provide a major source of ER for the growing bud. In fact, we never observed the cecER domain on the other side of the nucleus away from the bud or bud scars. It is informative to visualize ER domain organization during inheritance by separating the models for the cytoplasmic tubER and cecER away from the models for pmaER. The models of tubER and cecER show that these domains transition directly from the mother into the bud (Fig. 2, B–E, middle). In contrast, the pmaER shows no continuity through the bud neck in any of our models (Fig. 2, A–F, right). The pmaER is continuous with the tubER and cecER, and so, parts of this domain could also be inherited. However, if it is, it must first peel away from the PM and transition into tubER or cecER before passing through the bud neck. By the last stage of budding (Fig. 2 F), the pmaER is enriched in the mother, and both the cecER and tubER are reduced (Fig. 2, G and H). These structures demonstrate that the pmaER is not inherited through the bud neck.

ER domain inheritance into the bud

We characterized the structure, volume, and relative abundance of ER domains in the growing bud (Fig. 2, A–F, I, and J). Our smallest bud contains just the tips of ER tubules (Fig. 2 A). A slightly larger bud contains two ER tubules extending like fingers into the bud (Fig. 2 B, left, red arrow). These data are consistent with previous reports that ER tubules are the first domain inherited into the bud along the mother–bud axis (Du and Novick, 2001; Estrada de Martin et al., 2005a). The number of tubules continues to increase into a nexus of tubules as the bud grows (Fig. 2, C and D). A small region in the middle of the ER tubule nexus is the cecER in later buds (Fig. 2, D and E, yellow domain in the bud). The ER traverses through the bud neck initially along the mother–bud axis. However, at around the equator of the bud, ER tubules branch out toward the periphery to form PM contacts in multiple directions to reestablish pmaER domains (Fig. 2, C–F, blue pmaER contacts on left and right).

All ER domains have a similar range of diameters/widths

We measured and compared the dimensions of all three peripheral ER domains, including pmaER, cecER, and tubER, at about the resolution of the membrane bilayer (4 nm). This is the first time these dimensions have been measured and directly compared using high-resolution 3D tomography. Previous measurements have involved room temperature chemical fixation and a high percentage of fixatives prone to artifact and altered membrane shape (Murk et al., 2003) or are performed with 2D TEM. We first measured the dimensions of nine individual ER tubules (tubER) taken from six different cells that range in length from 250 to 700 nm (Fig. 3 A, each tubule is shown in a different color). Tubule diameters were measured as the distance

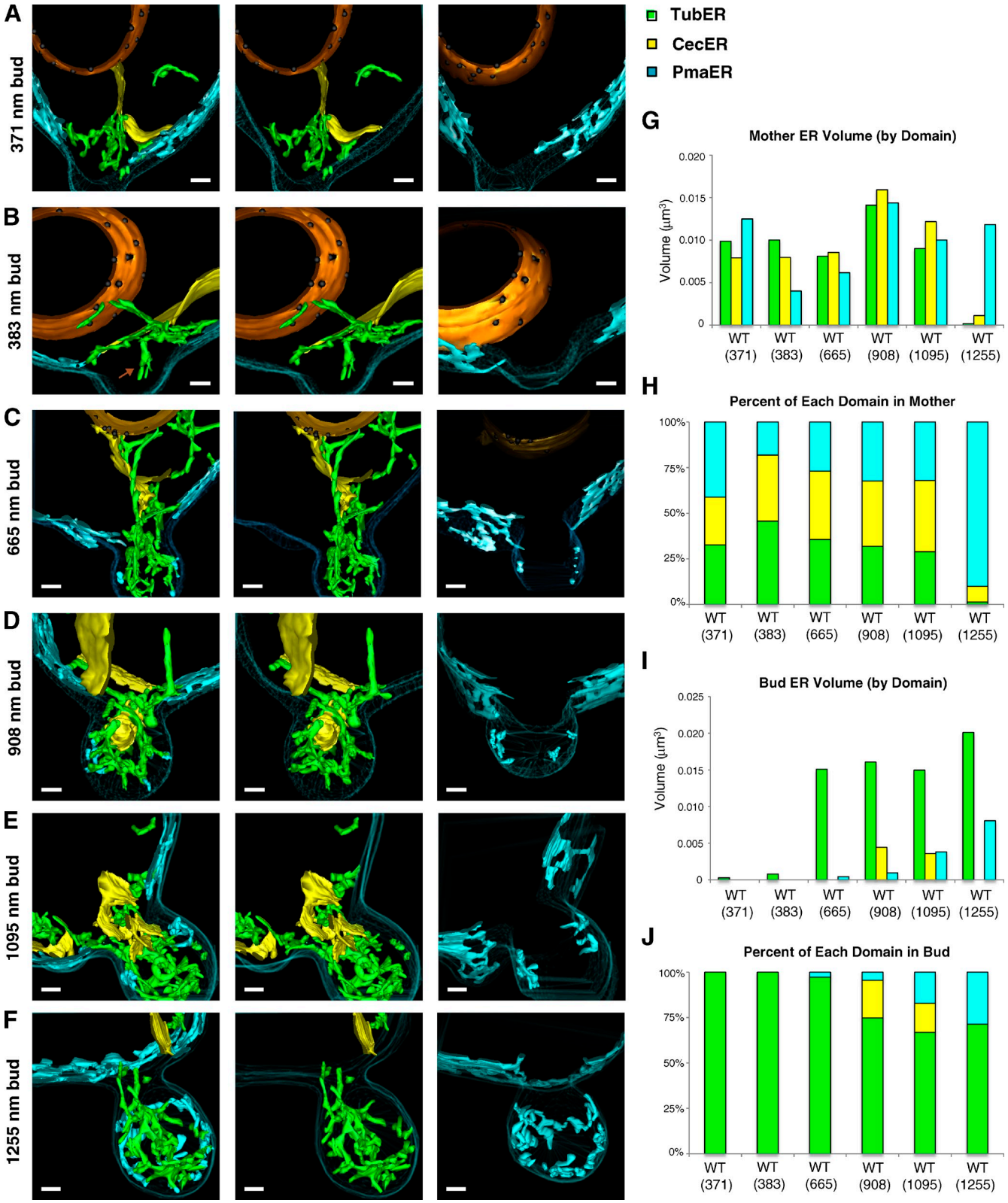

Figure 2. **3D ER domain distribution and abundance during inheritance.** (A–F) 3D models derived from 200-nm-thick section serial tomograms show ER domain organization in six different wt cells ordered by increasing bud sizes. Corresponding 2D tomographs are shown in Fig. S3 (A–F). Panels show domain distribution of all ER domains (left), cecER and tubER (yellow and green domains in middle), and pmaER alone (blue on right). (G) Graph of peripheral ER domain volumes found in reconstructed sections of cells in A–F. (H) Relative percentage of each domain in the mother cell for A–F. (I) As in G for the bud. (J) As in H for the bud ER. Bars, 200 nm.

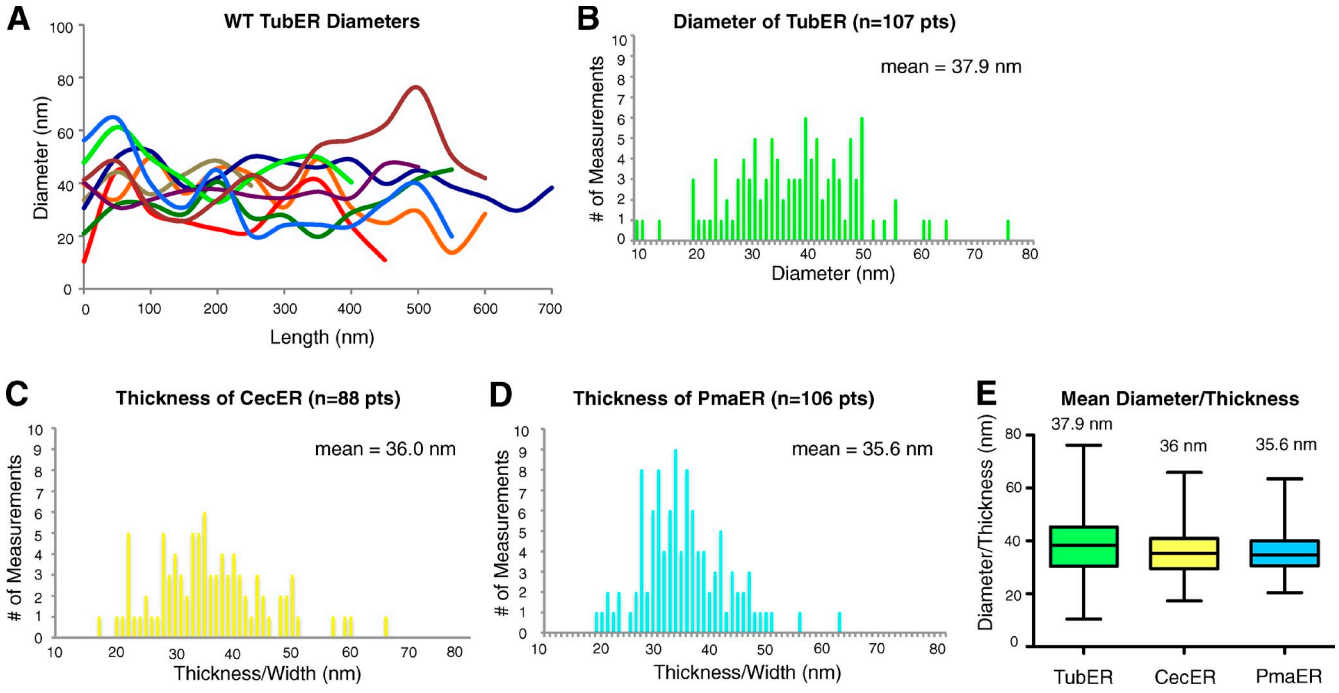

Figure 3. **Quantitative analysis of 3D ER domain dimensions.** (A) Nine individual wt ER tubules were measured at 50-nm intervals along their lengths. Tubule lengths range from ~250 to 700 nm; each tubule is shown in a different color. (B) Histogram showing the distribution of all tubER diameter measurements (n = 107 measurements taken from the nine tubules shown in A). (C) As in B for cecER thickness (n = 88 measurements). (D) As in B for pmaER thickness (n = 106 measurements). (E) Comparison of mean diameters/thickness for ER domains calculated from the data points shown in B–D. Brackets show range of measurements, and boxes show SEM. Horizontal lines show means given above the boxes.

from the outside surface of one side of the membrane bilayer perpendicular through the lumen to the outside surface of the opposing membrane bilayer. Diameters were measured every 50 nm along the length of each tubule, and all of the recorded measurements were graphed on a histogram, which shows a range from 10 to 76 nm (Fig. 3 B, mean diameter = 37.9 ± 1.1 nm, SEM; n = 107). These data demonstrate that tubules are rather unduloid in nature, but their diameters are maintained within a limited range.

We next determined the thickness of the cecER. cecER thickness was measured from the outside surface of one face of the cecER bilayer perpendicular through the lumen to the outside of the other face to include the thickness of both membrane bilayers and the lumenal spacing (Fig. 3 C). The thickness of six different cecER regions taken from five different cells was measured to obtain 88 measurements covering a total area of 0.168 μm^2. cecER thickness ranges from 17 to 66 nm (Fig. 3 C, mean width = 36.0 ± 1.0 nm, SEM; n = 88). The thickness of the pmaER was measured by the same method as for the cecER: from the PM face through the lumen to the outside of the cytosolic face. 12 separate pmaER domains coming from six different cells yielded n = 106 measurements covering a total area of 0.26 μm^2. These data were plotted and demonstrate that pmaER thickness ranges from 20 to 63 nm (Fig. 3 D, mean = 35.6 ± 0.7 nm, SEM). Others have reported a similar mean spacing of 31 nm for the cortical ER by 2D TEM analysis of HPF, FS samples (Bernales et al., 2006). Strikingly, the range and mean diameters/thickness of the tubER, pmaER, and cecER are almost identical (Fig. 3 E, 37.9, 35.6, and 36 nm, respectively).

All ER domains are restructured in the absence of Rtns and Yop1

Our data provide a baseline understanding of wt ER structure and organization in the mother and bud during multiple stages of early ER inheritance. We could then compare wt ER structures to mutant structures where tubule-shaping proteins (Rtn1, Rtn2, and DP1/Yop1) are absent to gain insight into how and where these proteins affect ER domain organization. These proteins affect tubER structure in yeast when assayed at the level of fluorescence microscopy (De Craene et al., 2006; Voeltz et al., 2006). However, recent images have shown that Rtns are also localized to the edges of ER cisternae, which are also regions with high membrane curvature (Kiseleva et al., 2007; Schuck et al., 2009; Shibata et al., 2010; Sparkes et al., 2010). We reasoned that a detailed 3D structure of ER organization in the absence of these tubule-shaping proteins could reveal whether they also shape membrane curvature at other ER domains, such as the edges of cisternae.

We solved two 3D EM structures of the ER in yeast cells lacking Rtn1, Rtn2, and Yop1 (*Δrtn1rtn2yop1*; Voeltz et al., 2006). Mutant cells were grown, HPF, FS, sectioned, reconstructed into tomograms, and modeled in 3D by the same methods described for wt. Two mutant ER structures are shown for cells with different bud sizes, and these structures can be compared with wt (Fig. 4, 595- or 1,253-nm mutant compared with 665- or 1,255-nm wt). Mutant tomographs and rotating 3D structures are also shown in Videos 7 and 8. We used these models to calculate the ER domain distribution, volume, and relative abundance in the mutant mother and bud and compared these values with those of wt cells (Fig. 4, E and F). As expected, the

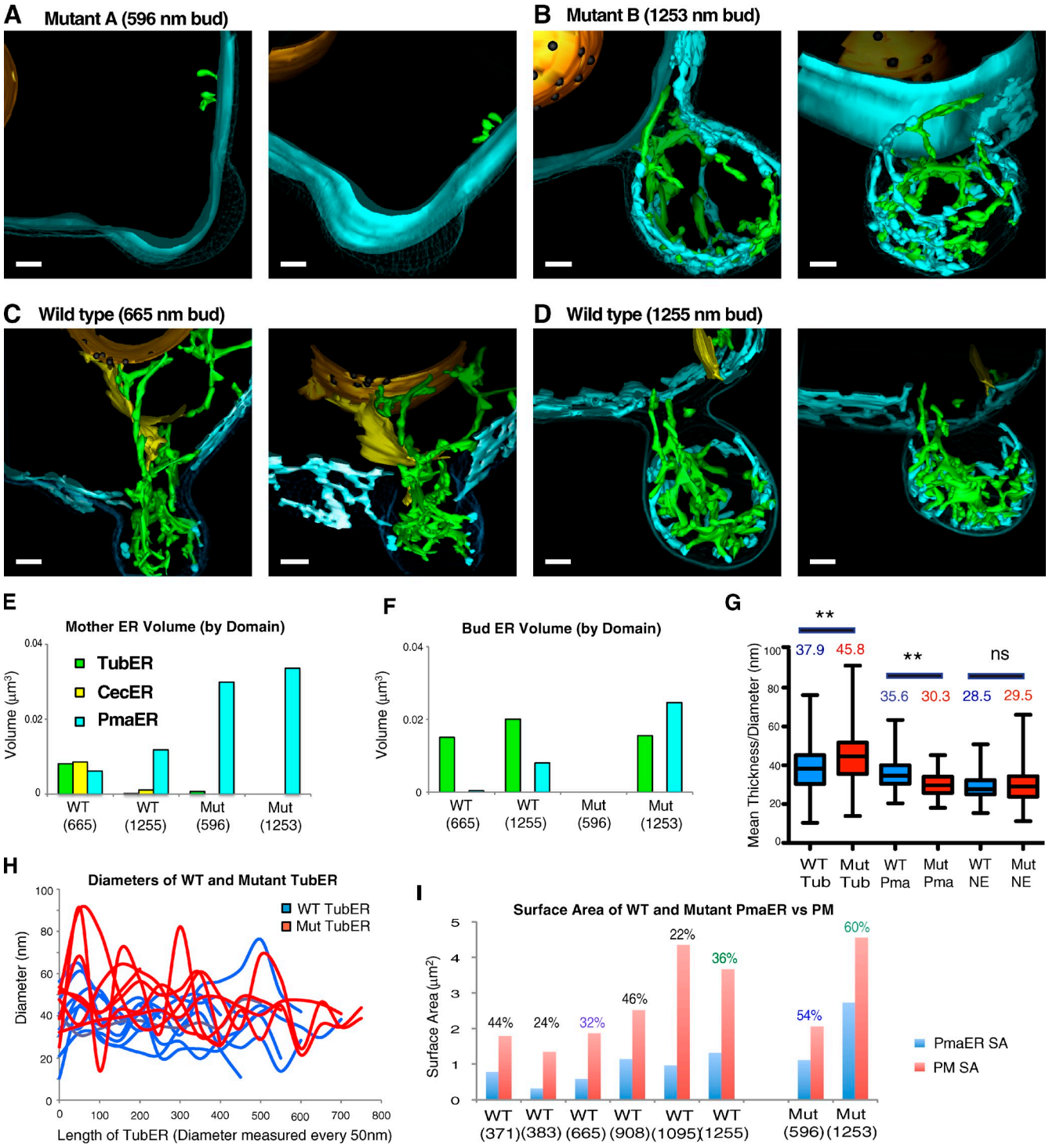

Figure 4. **3D ER domain structure in mutant *Δrtn1rtn2yop1*.** (A and B) 3D models showing ER domain organization at two different angles of a mutant cell (mutant = *Δrtn1rtn2yop1*) with a 596-nm bud (A) and a 1,253-nm bud (B). (C and D) 3D model of a wt cell with a 665-nm bud (C) and a 1,255-nm bud (D) to compare with mutants. All ER domains are color coded as in Fig. 1. (E) Graph comparing the volume of each peripheral ER domain found within the reconstructed volume of the mutant mother cell (in A and B) compared with that of wt cells (C and D) with similar bud sizes. (F) As in E for the bud. (G) Comparison of mean diameters for wt and mutant ER domains showing differences in diameters/thickness that are significant for tubER and pmaER but not for NE. Horizontal lines indicate mean diameters given above the boxes. Mutant tubER mean diameter = 45.8 ± 1.6 nm versus 37.9 ± 1.1 nm for wt; mutant pmaER mean thickness = 30.3 ± 0.44 nm versus 35.6 ± 0.74 nm in wt (both are significant by unpaired *t* test; **, P < 0.0001). NE mutant mean thickness = 29.5 ± 0.6 nm versus 28.5 ± 0.6 nm for wt (not significantly different; P = 0.28). Brackets show range of measurements, and boxes show SEM. (H) Lengthwise diameters of nine different wt tubules and seven different mutant tubules. (I) 3D models were used to calculate the surface area of pmaER and PM to determine the percentage of the PM covered by the pmaER for wt and mutant cells. Blue and green percentages show comparisons between the wt and mutant cells with similar bud sizes. Bud sizes are indicated below each graph. Mut, mutant. SA, surface area. Bars, 200 nm.

tubER is dramatically reduced in the mutant mother cells compared with wt (compare Fig. 4, A and C). The ER in both mutants in the mother cell was organized, instead, into an extensive pmaER domain that lacks both tubular regions and cisternal fenestrations (Fig. 4, A and B). We categorized this domain as pmaER instead of cecER because it is closely associated with the PM (except at the bud neck where it is lining the contour of the mother cell) and almost entirely ribosome excluded on its PM face. Also, in contrast to wt cells, we do not find any cytoplasmic cecER facing the bud in the mutant mother cell (Fig. 4, A, B, and E, graph). Indeed, the mutant mother cells lack all domains of membrane curvature, including (a) tubER domains in the cytoplasm, (b) tubER domains at the pmaER, and (c) fenestrations on the cisternae at the pmaER.

Our data demonstrate that all regions of membrane curvature in the peripheral ER are shaped by the Rtn/Yop1 proteins in yeast. Because all these domains also have similar diameters/thickness in wt cells, we next asked whether the dimensions of the peripheral ER would be altered in the absence of Rtns/Yop1. We measured the thickness of six different mutant pmaER domains by 3D tomography to obtain 162 measurements over a total surface area of 0.408 μm^2 (n = 5 different mutant cells). These data were graphed in a histogram to display the range of mutant pmaER thickness (Fig. S4 A). The mean diameter of mutant pmaER is narrower than wt pmaER (Fig. 4 G, mean = 30.3 ± 0.44 nm in mutant vs. 35.6 ± 0.74 nm in wt; a significant change of $P < 0.0001$ by unpaired t test). In contrast, Rtn/Yop1 deletion does not affect the mean thickness of the NE (Fig. 4 G, mean width = 28.5 ± 0.6 nm [SEM] for wt vs. 29.5 ± 0.6 nm [SEM] for mutant; not significantly different by unpaired t test, $P = 0.28$). Therefore, Rtn/Yop1 deletion does significantly alter the thickness of the pmaER cisternae but not of the NE.

If Rtns and Yop1 are the only proteins required to generate tubER, we would not expect to see tubER in the bud of the mutant. However, we find that the larger mutant bud contains both tubER and pmaER and a high degree of membrane curvature (Fig. 4 B). Therefore, the tubER is still being pulled out of the mutant mother cell pmaER into the bud by a process that does not initially require Rtns/Yop1. If Rtns/Yop1 are not required to make tubER but are instead required to stabilize them, we expected that the tubER domains in the mutant bud would have more irregular diameters than in wt. We therefore measured and compared the shape of mutant bud tubER with those of wt (Fig. 4 H, seven mutant tubules and nine wt tubules). We obtained 82 diameter measurements taken at 50-nm intervals along the length of the seven tubules taken from five different mutant cells to cover a total surface area of 0.203 μm^2 and determined the range of tubER diameters (Fig. S4 B, histogram). We find that the tubER in the mutant bud are even more unduloid and irregular than in wt (Fig. 4 H). As a result, the mean diameter of tubER in the mutant cells is wider than in wt cells (Fig. 4 G, diameter = 45.8 ± 1.6 nm [SEM] in mutant compared with 37.9 ± 1.1 nm [SEM] in wt; a significant difference by unpaired t test, $P < 0.0001$). Together, these data support a model whereby Rtns/Yop1 maintain/stabilize rather than generate the membrane curvature at tubER and at the edges of cisternae.

Rtn/Yop1 deletion increases the degree of contact between PM and pmaER

The resolution of our 3D images allows us to calculate the degree to which the PM is covered by pmaER. We measured the percentage of the PM that is tightly associated with pmaER by calculating the surface area of the (PM facing) pmaER and dividing this number by the surface area of modeled PM for each of our six wt structures. These calculations reveal that between 20 and 45% of the PM in wt cells (mother and bud included) is tightly associated with pmaER (Fig. 4 I; these data are similar to calculations predicted by fluorescence microscopy in Schuck et al., 2009). When Rtns/Yop1 are deleted, the peripheral ER is converted into a large cisterna in the mother cell that is unfenestrated and, yet, still tightly associated with the PM (Fig. 4, A, B, and E). As a result, mutant pmaER covers a larger surface area of PM than wt pmaER (Fig. 4 I, 54 and 60% coverage in the mutant with 596- and 1,253-nm buds compared with 32 and 36% coverage in the wt with 665- and 1,255-nm buds, respectively). Most of the surface area of the PM that is not covered by pmaER in the mutant is found in the bud. However, even in the mutant bud, the volume of pmaER is increased compared with that of a wt cell with a similar bud size (compare Fig. 4, B, D, and F, graph). Our data demonstrate, for the first time, that one role of Rtn/Yop1 and ER membrane curvature is to regulate the abundance of the pmaER domain.

Relationship between ER ribosome density, shape, and Rtns/Yop1

Our preservation techniques and the near molecular resolution of our 3D models of ER structure make it possible for us to probe the relationship between ER ribosome density, membrane shape, and ER localization. Specifically, what effect does membrane curvature have on ER ribosome density? Recently, the Rapoport laboratory has shown by comparing the fluorescence intensity of immunostained COS cells that several components of the translocation complex are enriched in cisternae versus tubules relative to luminal proteins (Shibata et al., 2010). However, the relative ribosome densities of these two differently shaped domains have never been directly compared in the same cell, nor has the ribosome density of the pmaER ever been measured. Here, we probe the relationship between ribosome density and ER domain structure by high-resolution EM and 3D tomography. We first marked all ribosomes bound to the ER membrane in our models (bound ribosomes are those within 5 nm of the membrane bilayer). Ribosomes appear in tomograms as darkly stained round objects (~10 nm in diameter) and are marked as dots colored as the domain to which they are bound (Fig. 1 C, example of ribosome bound to the ER marked by a red arrow). We have displayed models of four of our wt cells with each domain color coded as in Fig. 1 and with ER-bound ribosomes shown as small spheres that are colored to match the domain to which they are bound (Fig. 5, A–D, top and bottom show models at different angles). These models were used to then calculate the ribosome density over the surface area of each domain in the mother or the bud (Fig. 5, E and F, respectively). The cytoplasmic and PM faces of the pmaER were calculated independently because they have dramatically different ribosome densities. The pmaER membrane that faces the PM is shown in red bars

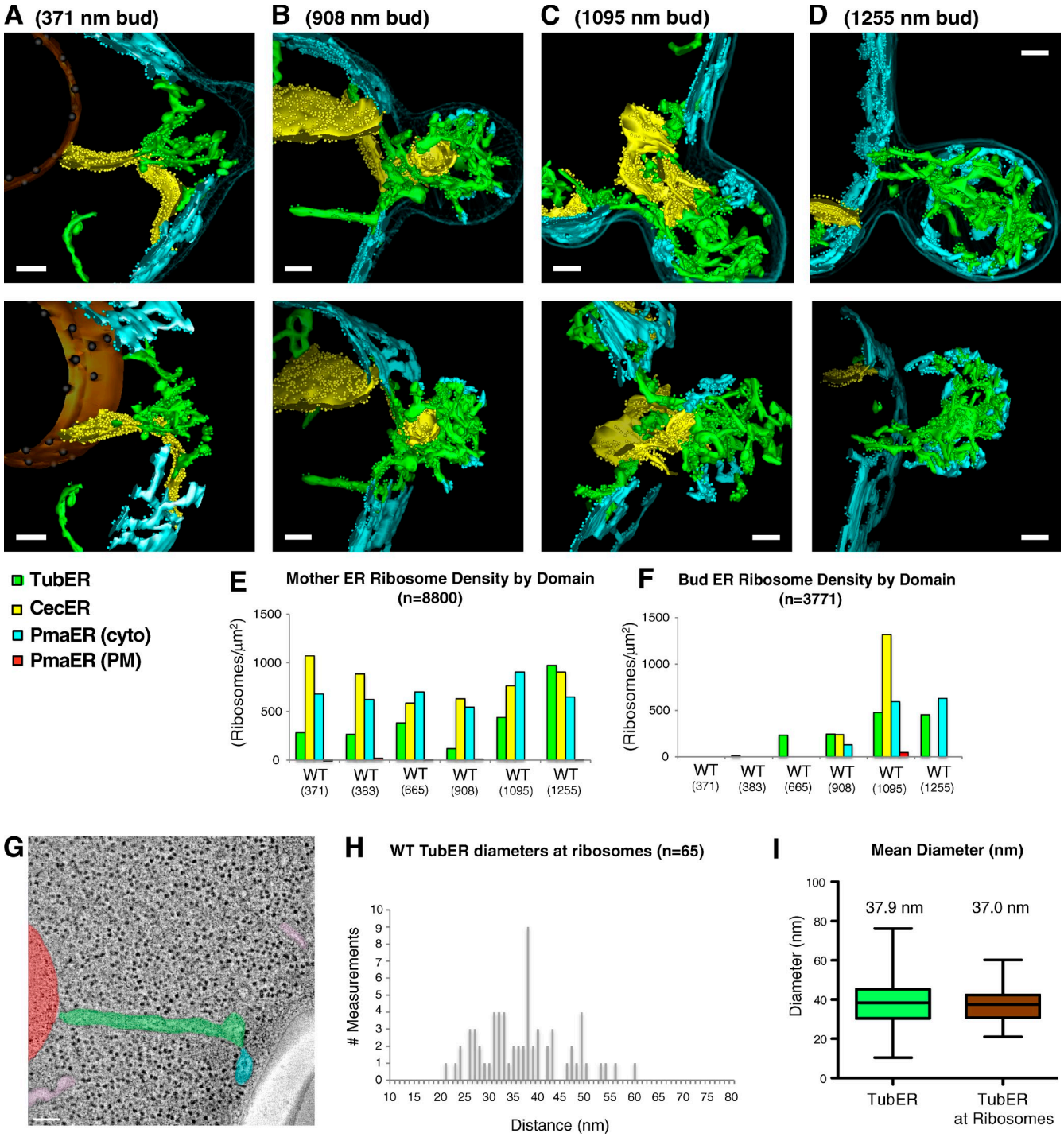

Figure 5. **ER domain ribosome density and distribution during inheritance.** (A–D) 3D models of wt cells in order of bud size (as indicated). ER domains are color coded as in Fig. 1, and ribosomes are indicated as dots in the color of the ER domain to which they are bound. (E) The number of ribosomes per surface area was calculated for each domain in each of the wt mother cells. Bud size is shown on the bottom. (F) As in E for the bud. (G) A magnified 2D tomograph shows an ER tubule that is contacting a vacuole (red). Note the apparent lack of ribosomes (black dots) on the membrane. (H) The histogram shows the range of ER tubule diameters at the positions where ribosomes are bound (n = 65). (I) The mean tubER diameter at which ribosomes are bound (37.0 ± 1.1 nm; n = 65) is compared with the overall mean tubER diameters in the tubER population (37.9 ± 1.09 nm, from Fig. 3 E; n = 107). Brackets show the ranges, and boxes show the SEM. Horizontal lines indicate the means. cyto, cytoplasmic face. Bars: (A–D) 200 nm; (G) 50 nm.

and is essentially ribosome excluded (Fig. 5, E and F). We show that cecER and the pmaER (cytoplasmic face) have the highest ribosome densities ranging from ~600 to 1,100 ribosomes/μm^2 for the cecER and ~550 to 900 ribosomes/μm^2 for the pmaER (cytoplasmic face). The ribosome density of yeast cecER is similar to that of mitotic mammalian BSC1 cell cisternae, which was determined by similar methods (1,000 ± 300 μm^2; Lu et al., 2009). The tubER is bound by ribosomes, although it does have less bound ribosomes than the other domains (typically ~250–400 ribosomes/μm^2 density for tubER; Fig. 5 E). ER ribosome

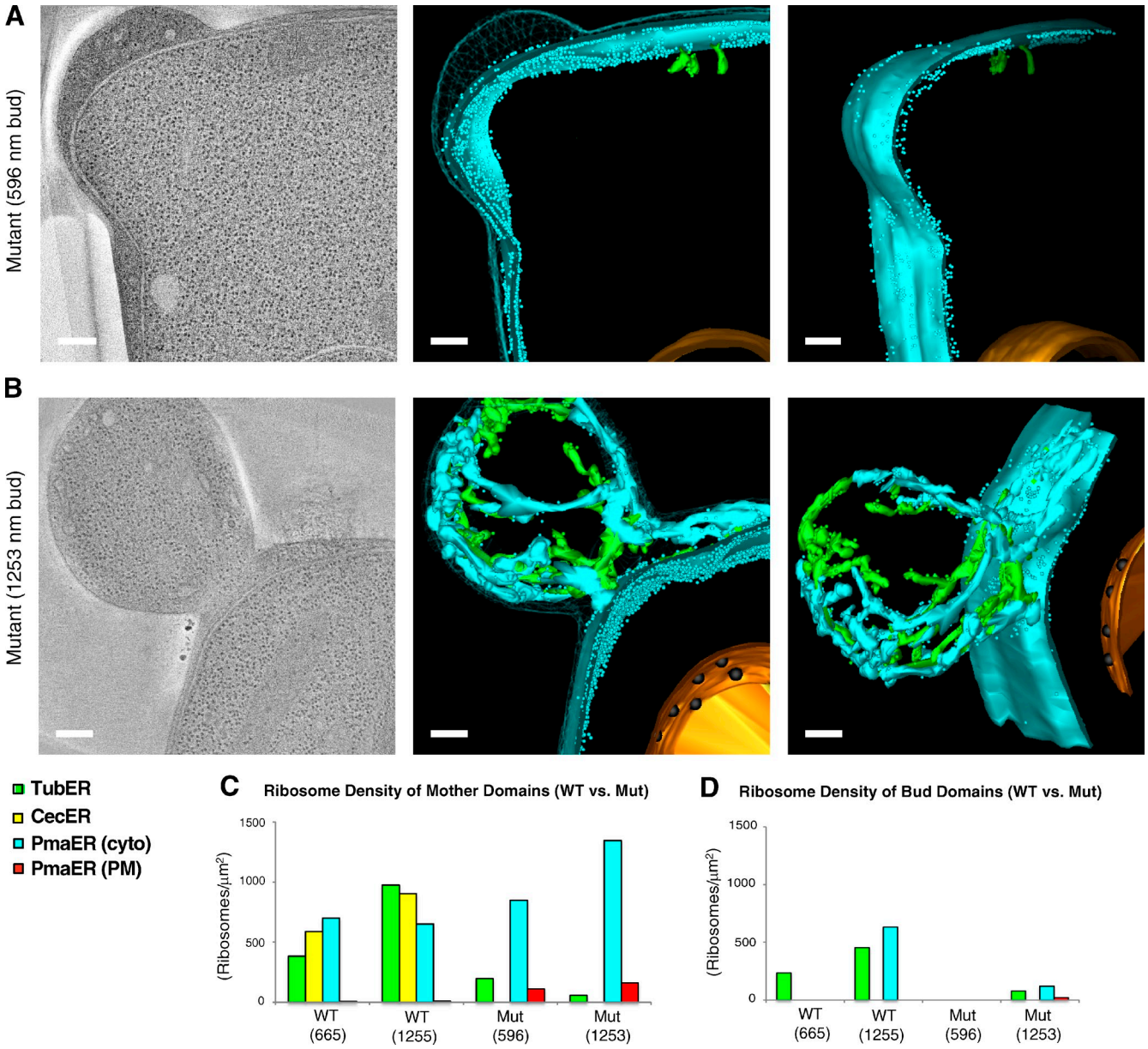

Figure 6. **ER domain ribosome density without Rtns/Yop1.** (A) 2D tomograph of a mutant cell with a 596-nm bud (left). Ribosomes are black dots. Note that the expansive pmaER membrane lacks tubules and fenestrations. (right) 3D model of ER domain organization in the mutant at two different angles. Peripheral ER domains are marked as in Fig. 1 with bound ribosomes indicated as dots in the color of the domain to which they are bound. (B) As in A for a mutant with a 1,253-nm bud diameter. (C) The number of ribosomes per surface area was calculated for each domain in the mother of a mutant and compared with wt cells; bud size is shown on the bottom. Domains are color coded as before with the cytoplasmic face (cyto) of pmaER in blue and PM face of pmaER in red. n = 6,511 mother ribosomes (wt = 2,044 and mutant = 4,467). (D) As in C for the bud. n = 2,029 bud ribosomes (wt = 1,727 and mutant = 302). Mut, mutant. Bars, 200 nm.

densities are generally lower in the bud than in the mother, suggesting that ribosomes may dissociate and then need to reassociate during inheritance (compare densities in Fig. 5, E and F). Together, these data demonstrate that tubER does have less bound ribosomes than cecER and pmaER. However, membrane curvature alone does not define ER ribosome density because pmaER and cecER have very similar levels of bound ribosomes.

tubER diameter does not restrict ribosome density

Occasionally, we find tubER domains that appear to be ribosome excluded. We show an example of one of these ER tubules that makes contact at its very tip with a vacuole (Fig. 5 G, ribosome exclusion zone around the membrane of this green tubule that is contacting a vacuole in red). Ribosome binding to the ER may be sensitive to membrane curvature, and if it is, we predicted that ribosomes would bind at a higher frequency to the wider regions of the tubules. To test this, we measured the tubER diameter at the positions where a ribosome is bound (for eight tubules). The tubule diameters at which ribosomes bind were plotted as a histogram (Fig. 5 H). This distribution is very similar to the histogram for tubER diameters in the measured population and shows no obvious preference for wider diameters (Fig. 5 I, mean diameter = 37.0 ± 1.1 nm [SEM] for ribosomes [n = 65] vs. 37.9 ± 1.09 nm

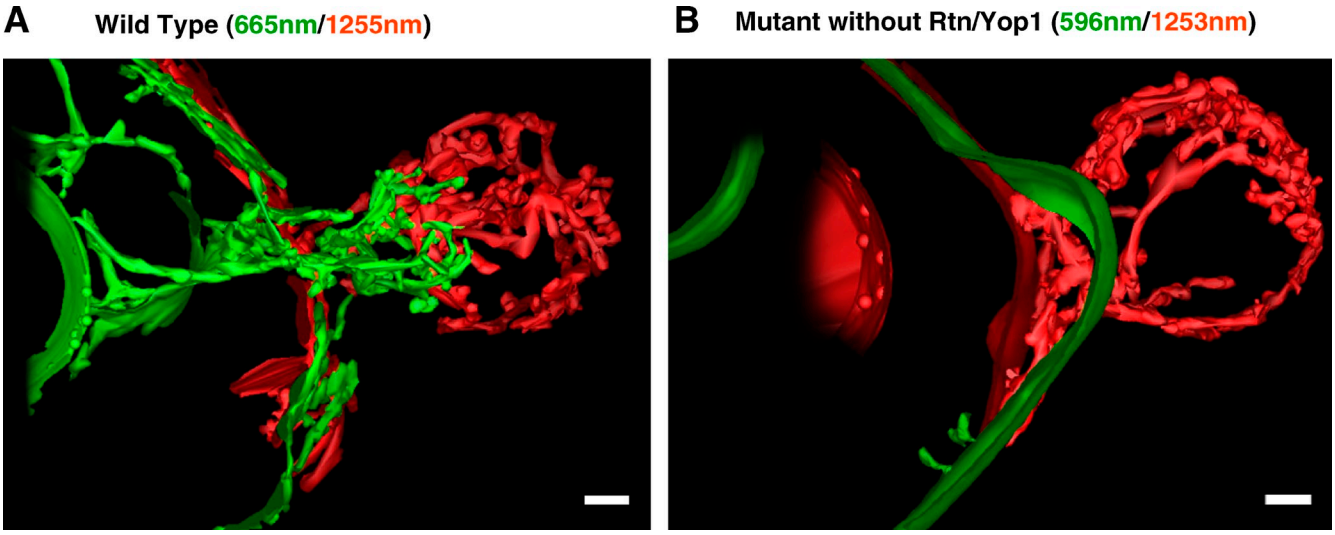

Figure 7. **Dramatic changes in ER shape and curvature occur in the absence of Rtns/Yop1.** (A) 3D model of ER in a wt cell with a 665-nm bud and a 1,255-nm bud that were overlayed to show the transition of ER domains into the bud. (B) As in A for corresponding mutant cells. Note the loss of membrane curvature throughout the mother of both mutant cells. However, the ER is still inherited by an Rtn/Yop1-independent process into the bud. Bars, 200 nm.

[SEM] for the tubER population [n = 107]; not significant by unpaired t test). Therefore, ribosomes are not restricted to the wider and less curved regions on ER tubules, which suggests that factors other than membrane curvature are aiding to exclude ribosomes from binding to tubER.

Deletion of Rtn/Yop1 alters ribosome density on the ER

We next tested whether Rtn/Yop1 deletion affects the ribosome density of the ER. We show thin-section 2D tomographs of mutant cells with nicely contrasted ribosomes throughout the cytoplasm and on the ER (Fig. 6 A and B, left, ribosomes are black dots). We marked all ribosomes on these models as small circles in the color of the domain to which they are bound (Fig. 6, A and B, middle and right show two different angles). We then measured the ribosome density of all peripheral ER domains in the two mutants and compared these with the corresponding wt cells (Fig. 6, C and D). The ribosome density of the cytoplasmic face of the pmaER in the smaller mutant mother cell was only slightly higher than the ribosome density of the wt pmaER, suggesting that the lack of membrane curvature or the lack of Rtns/Yop1 alone is not sufficient to dramatically increase ribosome density (Fig. 6 C, compare blue bars in the 596-nm mutant with the 665-nm wt cell). However, in the larger mutant mother cell (Fig. 6 B), the ribosome density of the pmaER is dramatically increased (1,347 vs. 651 ribosomes/μm^2 in the mutant and the wt, respectively; Fig. 6 C). We also measured the ribosome density of the tuber that is present in the bud of the larger mutant (Fig. 6 D). The ribosome density of the tubER in the mutant bud is reduced when compared with wt tubER (Fig. 6 D). Therefore, deletion of Rtn1/Yop1 actually decreases the ribosome density on the tubER, and Rtns/Yop1 are not responsible for physically excluding the ribosomes from binding to the tubules. Because the tubER in the mutant bud is wider overall than in the wt, these data further support the notion that membrane curvature is not limiting ribosome density on tubules. The pmaER in the mutant bud also has a dramatically decreased ribosome density compared with the wt bud. These data show that Rtns/Yop1 and membrane curvature play a role in distributing ribosome density throughout the ER and during inheritance.

We have overlayed two 3D models of the ER in a wt cell at different stages of inheritance (Fig. 7 A, the ER is green for the small bud and red for the large bud). We can compare these models with those of mutant cells lacking Rtns/Yop1 (Fig. 7 B). These models reveal that Rtn1/Yop1 proteins maintain membrane curvature throughout the peripheral ER, and their deletion changes multiple aspects of ER organization, including ER shape, distribution, inheritance, PM association, and ribosome density.

Discussion

We solved and analyzed by EM and tomographic 3D reconstruction the architecture of the peripheral ER during six stages of budding to establish a baseline of ER organization. The resolution in the tomograms (~4 nm) was sufficient to resolve membrane bilayers and bound ribosomes. Our images reveal that the ER in yeast is divided into three structurally distinct major domains: the pmaER, cecER, and tubER (Fig. 1). The cecER is a previously uncharacterized ER domain. It is unfenestrated, bound by ribosomes on both sides, and is present in five of our six reconstructed cells. We only observed the cecER in the quadrant of the cell that faces the bud, suggesting that this domain could have an exclusive role in ER inheritance. Our analysis of tubER reveals that it is not perfectly cylindrical; diameters vary along the length of individual tubules (Fig. 3, A and B). The diameter of tubER is, however, maintained within a range, suggesting that Rtns/Yop1 can be organized to structure a range of curvatures (which fall somewhere between 10 and 75 nm). The pmaER has many surprising features. It is made up of both tubules and fenestrated cisternae, which are so tightly linked to the PM that ribosomes are excluded between the two membranes (Fig. 1, E–G). The pmaER covers ~20–40% of the

PM in wt cells (varies with bud size; Fig. 4 H). Direct contacts between the PM and pmaER membranes can occasionally be found when we search for them (Fig. S5 A). Together, these data reveal a large pmaER–PM domain that may be unavailable for processes like vesicle-directed endocytosis and secretion. Indeed, within our tomograms, we have only observed invaginations of the PM at regions of the PM that are not bound by the ER (for an example see Fig. S5 B). The proteins that maintain this pmaER–PM domain have not been identified.

We have established at an unprecedented spatial resolution the features that peripheral ER domains share and the ones that are distinctly different (Figs. 2 and 3). Our experiments show that all peripheral ER domains have similar diameters/thickness (Fig. 3 E). These data indicate that they might all be organized by some of the same membrane-shaping proteins. Indeed, we found that mother cells lacking Rtns/Yop1 were dramatically depleted of tubules and all other peripheral ER regions of membrane curvature, including fenestrations and other cisternal edges (Figs. 4 and 7). Several studies have localized Rtns in multiple eukaryotes to the edges of cisternae (Kiseleva et al., 2007; Schuck et al., 2009; Shibata et al., 2010; Sparkes et al., 2010). Our data now reveal, for the first time, that the deletion of Rtn and Yop1 proteins also decreases the amount of curvature found at cisternae, which leads to a loss of cecER and a loss of pmaER cisternal fenestrations (Fig. 4). High-resolution 3D structural analyses of the Rtn1 or Yop1 complex by EM or x-ray crystallography will be required to confirm how these proteins organize along the curved edges of both cisternae and tubules.

The resolution of our 3D models allowed us to visualize the positions of individual ribosomes on each of the ER domains and probe the relationship between membrane curvature and ribosome density. Recent data from the Rapoport laboratory have shown using confocal fluorescence microscopy of immunostained mammalian COS cells that components of the translocation complex are enriched in cisternae relative to tubules, which indicates that the cisternae may have more bound ribosomes per surface area (Shibata et al., 2010). We directly measured the ribosome density of ER domains and similarly found that cecER has a higher ribosome density than tubER in yeast. tubER does have ribosomes bound to it, just at a lower density than does cecER. However, our data suggest that the reduced ribosome density of tubER is not caused by membrane curvature alone because we did not find an inverse correlation between tubER diameter and ribosome density (Fig. 4 I). We have also determined, for the first time, the ribosome density of the pmaER. The ribosome density of the pmaER is similar to that of cecER even though pmaER has a high degree of membrane curvature. Together, these data indicate that membrane curvature is not the major determinant of ribosome density. We further determined the effect of Rtn/Yop1 depletion on ribosome density, and we find that ribosome density changes dramatically in the absence of these membrane-shaping proteins in yeast (Fig. 6).

We used our 3D models to define the organization of the ER during early stages of ER inheritance. ER tubules are inherited first into the bud, initially along the mother–bud axis as previously suggested (Du and Novick, 2001; Estrada de Martin et al., 2005b). Our work additionally reveals that the source of the inherited ER is from the mother cecER and tubER domains and not from the pmaER. The data supporting this model are (a) the pmaER is completely excluded from the bud neck in all six of our models, (b) the inherited ER is directly continuous with the mother cell cecER and tubER, (c) the cecER and tubER are depleted from the mother cell as the bud grows, whereas the pmaER domain is not, and (d) the pmaER is reestablished at the bud PM by the tips of inherited cytoplasmic tubER. It is likely that the pmaER is not inherited because it is attached to the PM and/or because it cannot transition past the septin ring (Luedeke et al., 2005). Others report that inherited tubER is pulled into the bud along the mother–bud axis by myosin and actin until they attach to the far end of the bud PM, and then, the cortical ER spreads from the tip of the bud (Du et al., 2001, 2004, 2006; Fehrenbacher et al., 2002; Estrada et al., 2003; Wiederkehr et al., 2003). We do not see an accumulation of ER at the bud tip. Instead, the tubER accumulates into a nexus of tubules in the middle of the bud that then branches out to form new contacts in multiple directions with the PM to reestablish pmaER (Fig. 2, A–F).

Our analysis of ER inheritance revealed an important detail about the role of Rtns/Yop1 because we found that ER tubules are pulled out of the mother cisternae into the bud by a process that initially does not require Rtns/Yop1. Presumably, the ER tubules are still being pulled into the bud in the mutant by actin and Myo4p and the exocyst (Estrada de Martin et al., 2005a). However, these ER tubules were significantly larger in the mutant bud compared with wt. The bloated appearance of the mutant bud tubER and the near absence of any membrane curvature in the mother cell are consistent with a model that Rtns/Yop1 stabilize and maintain regions of membrane curvature rather than generate them in yeast. These data complement the studies in animal cells that have shown that MT depolymerization converts the tubER into cisternae despite the presence of endogenous Rtns (Terasaki et al., 1986; Shibata et al., 2008; Lu et al., 2009).

An unexpected result of our work is that Rtns/Yop1 and membrane curvature regulate the amount of pmaER that covers the PM. In the absence of Rtns and Yop1, the mother cell pmaER is converted into a single large ER cisternae that lacks fenestrations and tubules and covers a larger percentage of the PM surface area than it does in wt cells (Fig. 4 I). It is somewhat surprising to us that this massive flat cisterna is now held up against the PM rather than existing simply as a cytoplasmic cisterna. Indeed, this mutant morphology is reminiscent of animal cells in which the mitotic ER is converted almost entirely into extended cisternae that lack membrane curvature and also appear to be held up against the PM (McCullough and Lucocq, 2005; Lu et al., 2009). Very little is known about the structure and function of the pmaER domain. It has been proposed to be involved in lipid and cholesterol trafficking (Prinz, 2007). Covering the PM with the ER could have dramatic affects on processes that occur on the PM, and these processes may need to be regulated throughout the cell cycle. Many questions requiring further EM and tomography remain, including how extensive is this pmaER–PM domain in other eukaryotic cell types, why would ER membrane curvature regulate the abundance of this domain, and how else is it regulated?

Materials and methods

Haploid *S. cerevisiae* cells (wt = BY4742 mat α or mutant = NDY257 mat α; Voeltz et al., 2006) were harvested at log phase, vacuum filtered on 0.45-µm Millipore paper, loaded into 0.25-mm aluminum hats, and HPF in a high pressure freezer (HPM 010; Balzers Union AG) as previously described (Nickerson et al., 2010). We used an automatic freeze substitution unit (AFS; Leica) for the freeze substitution with 0.1% uranyl acetate and 0.25% glutaraldehyde in anhydrous acetone (Giddings, 2003) embedded in embedding media (Lowicryl HM20; Polysciences) and polymerized at −60°C. An ultramicrotome (Leica) was used to cut 80-nm serial thin sections and 200-nm serial semithick sections, and sections were collected onto 1% Formvar films adhered to rhodium-plated copper grids (Electron Microscopy Sciences). Grids were placed sample-side down onto a fresh 1% Formvar film (Formvar sandwich), and both sides were labeled with fiduciary 15-nm colloidal gold (British Biocell International). The Formvar sandwich stabilized the sections, minimized peripheral shrinkage from the electron beam exposure, minimized fiducial gold artifacts, and produced equivalent z shrinkage from section to section (z scale = 1.4). Dual-axis tilt series were collected from the samples from ±60° with 1° increments at 300 kV using SerialEM (Mastronarde, 1997) at 300 kV using a field emission gun (Tecnai 30; FEI). Negative defocus equivalent to the sample thickness (~300 nm with the Formvar sandwich) was used after the autofocus to increase the phase-contrast component (fiducial gold measurements were used as a control). Tilt series were recorded at a magnification of 23,000× using SerialEM (Mastronarde, 2005). After 2x binning on the recording 4098 x 4098–pixel charge-coupled device camera (Megascan 795; Gatan, Inc.), this magnification creates a 2000 x 2000–pixel image with a pixel size of 1.02 nm on the specimen. The nominal resolution in our tomograms was ~4 nm, based upon section thickness, number of tilts, tilt increments, and tilt angle range (Crowther relation; Koster et al., 1997).

The IMOD package (Kremer et al., 1996) and its newest viewer, 3DMOD 4.0.11, were used to construct individual tomograms. These tomograms were then merged together in x, y, and z directions to obtain a large continuous volume. 3DMOD modeling software was used for the assignment of the outer leaflet of organelle membrane contours, and best-fit sphere models of the outer leaflet were used for vesicle measurements (O'Toole et al., 2002). All membrane structures were manually assigned to reconstruct and account for the membrane-bound compartments within the combined sections. IMODINFO provided the surface area and volume data of contour models. The PM half of the surface area of the pmaER was divided by the surface area of the PM for each mother and bud present in the tomogram to quantify the percentage of the pmaER surface covering the PM. In the mutants, the portion of the pmaER surface spanning the neck was subtracted from the PM-facing surface of the pmaER, and this new total was divided by the surface area of the PM. Diameters and distances were measured from the outer membrane leaflets at optimal xy orientations in the tomograms at 50-nm intervals using 3DMOD. ER tubules were measured at the orientation showing maximum diameter. ER cisternae were measured at the orientation showing minimal thickness. Ribosome density was calculated by counting the number of ribosomes over the ER surface area (ribosomes per square micrometer). Images were further enhanced and manipulated in Photoshop 7 (Adobe). We sorted, analyzed, and graphed data using Excel (Microsoft) for Mac 2008 (Apple) and Prism 5 (GraphPad Software) for Mac OS X (Apple). Videos were made in 3DMOD and assembled in QuickTime Pro 7.5 (Apple), and the video size was reduced to <10 MB by saving videos as an HD 720p in QuickTime.

Online supplemental material

Fig. S1 shows how bud sizes were measured. Fig. S2 shows tomographs and 3D models of ER domains, vesicles, and Golgi in wt cells. Fig. S3 shows vesicles in close proximity (within 10 nm) of the ER membrane. Fig. S4 shows the histogram of thickness/diameter measurements for the mutant pmaER and tubER. Fig. S5 shows tomographs of the contact site between the pmaER and PM and an invagination site at the PM that does not occur at PM–pmaER contacts. Videos1–6 show original tomographs and rotating 3D models of the six wt cells in order of bud size. Videos 7 and 8 show original tomographs and rotating 3D models of 596- and 1,253-nm mutant cells. Online supplemental material is available at http://www.jcb.org/cgi/content/full/jcb.201011039/DC1.

We thank J. Friedman, T. Giddings Jr., D. Mastronarde, G. Odorizzi, E. O'Toole, A. Staehelin, M. Winey, and the Boulder 3D Electron Microscopy facility for assistance with EM processing, shared equipment, and helpful suggestions.

This work is funded by the National Institutes of Health (RO1 GM083977 to G.K. Voeltz), a Searle Scholar Award (to G.K. Voeltz), and a National Institutes of Health predoctoral training grant (GM07135 to N. Zurek). A. Hoenger was supported by a grant from the National Center for Research Resources (P41-RR000592).

Submitted: 8 November 2010
Accepted: 22 March 2011

References

Achleitner, G., B. Gaigg, A. Krasser, E. Kainersdorfer, S.D. Kohlwein, A. Perktold, G. Zellnig, and G. Daum. 1999. Association between the endoplasmic reticulum and mitochondria of yeast facilitates interorganelle transport of phospholipids through membrane contact. *Eur. J. Biochem.* 264:545–553. doi:10.1046/j.1432-1327.1999.00658.x

Anderson, D.J., and M.W. Hetzer. 2008. Reshaping of the endoplasmic reticulum limits the rate for nuclear envelope formation. *J. Cell Biol.* 182:911–924. doi:10.1083/jcb.200805140

Audhya, A., A. Desai, and K. Oegema. 2007. A role for Rab5 in structuring the endoplasmic reticulum. *J. Cell Biol.* 178:43–56. doi:10.1083/jcb.200701139

Bernales, S., K.L. McDonald, and P. Walter. 2006. Autophagy counterbalances endoplasmic reticulum expansion during the unfolded protein response. *PLoS Biol.* 4:e423. doi:10.1371/journal.pbio.0040423

De Craene, J.O., J. Coleman, P. Estrada de Martin, M. Pypaert, S. Anderson, J.R. Yates III, S. Ferro-Novick, and P. Novick. 2006. Rtn1p is involved in structuring the cortical endoplasmic reticulum. *Mol. Biol. Cell*. 17:3009–3020. doi:10.1091/mbc.E06-01-0080

Du, L.L., and P. Novick. 2001. Yeast rab GTPase-activating protein Gyp1p localizes to the Golgi apparatus and is a negative regulator of Ypt1p. *Mol. Biol. Cell*. 12:1215–1226.

Du, Y., M. Pypaert, P. Novick, and S. Ferro-Novick. 2001. Aux1p/Swa2p is required for cortical endoplasmic reticulum inheritance in *Saccharomyces cerevisiae*. *Mol. Biol. Cell*. 12:2614–2628.

Du, Y., S. Ferro-Novick, and P. Novick. 2004. Dynamics and inheritance of the endoplasmic reticulum. *J. Cell Sci.* 117:2871–2878. doi:10.1242/jcs.01286

Du, Y., L. Walker, P. Novick, and S. Ferro-Novick. 2006. Ptc1p regulates cortical ER inheritance via Slt2p. *EMBO J.* 25:4413–4422. doi:10.1038/sj.emboj.7601319

English, A.R., N. Zurek, and G.K. Voeltz. 2009. Peripheral ER structure and function. *Curr. Opin. Cell Biol.* 21:596–602. doi:10.1016/j.ceb.2009.04.004

Estrada, P., J. Kim, J. Coleman, L. Walker, B. Dunn, P. Takizawa, P. Novick, and S. Ferro-Novick. 2003. Myo4p and She3p are required for cortical ER inheritance in *Saccharomyces cerevisiae*. *J. Cell Biol.* 163:1255–1266. doi:10.1083/jcb.200304030

Estrada de Martin, P., P. Novick, and S. Ferro-Novick. 2005a. The organization, structure, and inheritance of the ER in higher and lower eukaryotes. *Biochem. Cell Biol.* 83:752–761. doi:10.1139/o05-159

Estrada de Martin, P., Y. Du, P. Novick, and S. Ferro-Novick. 2005b. Ice2p is important for the distribution and structure of the cortical ER network in *Saccharomyces cerevisiae*. *J. Cell Sci.* 118:65–77. doi:10.1242/jcs.01583

Fehrenbacher, K.L., D. Davis, M. Wu, I. Boldogh, and L.A. Pon. 2002. Endoplasmic reticulum dynamics, inheritance, and cytoskeletal interactions in budding yeast. *Mol. Biol. Cell*. 13:854–865. doi:10.1091/mbc.01-04-0184

Friedman, J.R., B.M. Webster, D.N. Mastronarde, K.J. Verhey, and G.K. Voeltz. 2010. ER sliding dynamics and ER–mitochondrial contacts occur on acetylated microtubules. *J. Cell Biol.* 190:363–375. doi:10.1083/jcb.200911024

Giddings, T.H. 2003. Freeze-substitution protocols for improved visualization of membranes in high-pressure frozen samples. *J. Microsc.* 212:53–61. doi:10.1046/j.1365-2818.2003.01228.x

Grigoriev, I., S.M. Gouveia, B. van der Vaart, J. Demmers, J.T. Smyth, S. Honnappa, D. Splinter, M.O. Steinmetz, J.W. Putney Jr., C.C. Hoogenraad, and A. Akhmanova. 2008. STIM1 is a MT-plus-end-tracking protein involved in remodeling of the ER. *Curr. Biol.* 18:177–182. doi:10.1016/j.cub.2007.12.050

Höög, J.L., C. Schwartz, A.T. Noon, E.T. O'Toole, D.N. Mastronarde, J.R. McIntosh, and C. Antony. 2007. Organization of interphase microtubules in fission yeast analyzed by electron tomography. *Dev. Cell*. 12:349–361. doi:10.1016/j.devcel.2007.01.020

Hu, J., Y. Shibata, C. Voss, T. Shemesh, Z. Li, M. Coughlin, M.M. Kozlov, T.A. Rapoport, and W.A. Prinz. 2008. Membrane proteins of the endoplasmic reticulum induce high-curvature tubules. *Science*. 319:1247–1250. doi:10.1126/science.1153634

Kiseleva, E., K.N. Morozova, G.K. Voeltz, T.D. Allen, and M.W. Goldberg. 2007. Reticulon 4a/NogoA locates to regions of high membrane curvature and

may have a role in nuclear envelope growth. *J. Struct. Biol.* 160:224–235. doi:10.1016/j.jsb.2007.08.005

Koster, A.J., R. Grimm, D. Typke, R. Hegerl, A. Stoschek, J. Walz, and W. Baumeister. 1997. Perspectives of molecular and cellular electron tomography. *J. Struct. Biol.* 120:276–308. doi:10.1006/jsbi.1997.3933

Kremer, J.R., D.N. Mastronarde, and J.R. McIntosh. 1996. Computer visualization of three-dimensional image data using IMOD. *J. Struct. Biol.* 116:71–76. doi:10.1006/jsbi.1996.0013

Lee, C., and L.B. Chen. 1988. Dynamic behavior of endoplasmic reticulum in living cells. *Cell*. 54:37–46. doi:10.1016/0092-8674(88)90177-8

Lu, L., M.S. Ladinsky, and T. Kirchhausen. 2009. Cisternal organization of the endoplasmic reticulum during mitosis. *Mol. Biol. Cell*. 20:3471–3480. doi:10.1091/mbc.E09-04-0327

Luedeke, C., S.B. Frei, I. Sbalzarini, H. Schwarz, A. Spang, and Y. Barral. 2005. Septin-dependent compartmentalization of the endoplasmic reticulum during yeast polarized growth. *J. Cell Biol.* 169:897–908. doi:10.1083/jcb.200412143

Marsh, B.J., N. Volkmann, J.R. McIntosh, and K.E. Howell. 2004. Direct continuities between cisternae at different levels of the Golgi complex in glucose-stimulated mouse islet beta cells. *Proc. Natl. Acad. Sci. USA*. 101:5565–5570. doi:10.1073/pnas.0401242101

Mastronarde, D.N. 1997. Dual-axis tomography: an approach with alignment methods that preserve resolution. *J. Struct. Biol.* 120:343–352. doi:10.1006/jsbi.1997.3919

Mastronarde, D.N. 2005. Automated electron microscope tomography using robust prediction of specimen movements. *J. Struct. Biol.* 152:36–51. doi:10.1016/j.jsb.2005.07.007

McCullough, S., and J. Lucocq. 2005. Endoplasmic reticulum positioning and partitioning in mitotic HeLa cells. *J. Anat.* 206:415–425. doi:10.1111/j.1469-7580.2005.00407.x

Murk, J.L., G. Posthuma, A.J. Koster, H.J. Geuze, A.J. Verkleij, M.J. Kleijmeer, and B.M. Humbel. 2003. Influence of aldehyde fixation on the morphology of endosomes and lysosomes: quantitative analysis and electron tomography. *J. Microsc.* 212:81–90. doi:10.1046/j.1365-2818.2003.01238.x

Nickerson, D.P., M. West, R. Henry, and G. Odorizzi. 2010. Regulators of Vps4 ATPase activity at endosomes differentially influence the size and rate of formation of intralumenal vesicles. *Mol. Biol. Cell*. 21:1023–1032. doi:10.1091/mbc.E09-09-0776

O'Toole, E.T., M. Winey, J.R. McIntosh, and D.N. Mastronarde. 2002. Electron tomography of yeast cells. *Methods Enzymol.* 351:81–95. doi:10.1016/S0076-6879(02)51842-5

Pichler, H., B. Gaigg, C. Hrastnik, G. Achleitner, S.D. Kohlwein, G. Zellnig, A. Perktold, and G. Daum. 2001. A subfraction of the yeast endoplasmic reticulum associates with the plasma membrane and has a high capacity to synthesize lipids. *Eur. J. Biochem.* 268:2351–2361. doi:10.1046/j.1432-1327.2001.02116.x

Preuss, D., J. Mulholland, C.A. Kaiser, P. Orlean, C. Albright, M.D. Rose, P.W. Robbins, and D. Botstein. 1991. Structure of the yeast endoplasmic reticulum: localization of ER proteins using immunofluorescence and immunoelectron microscopy. *Yeast*. 7:891–911. doi:10.1002/yea.320070902

Prinz, W.A. 2007. Non-vesicular sterol transport in cells. *Prog. Lipid Res.* 46:297–314. doi:10.1016/j.plipres.2007.06.002

Prinz, W.A., L. Grzyb, M. Veenhuis, J.A. Kahana, P.A. Silver, and T.A. Rapoport. 2000. Mutants affecting the structure of the cortical endoplasmic reticulum in *Saccharomyces cerevisiae*. *J. Cell Biol.* 150:461–474. doi:10.1083/jcb.150.3.461

Puhka, M., H. Vihinen, M. Joensuu, and E. Jokitalo. 2007. Endoplasmic reticulum remains continuous and undergoes sheet-to-tubule transformation during cell division in mammalian cells. *J. Cell Biol.* 179:895–909. doi:10.1083/jcb.200705112

Schuck, S., W.A. Prinz, K.S. Thorn, C. Voss, and P. Walter. 2009. Membrane expansion alleviates endoplasmic reticulum stress independently of the unfolded protein response. *J. Cell Biol.* 187:525–536. doi:10.1083/jcb.200907074

Shibata, Y., G.K. Voeltz, and T.A. Rapoport. 2006. Rough sheets and smooth tubules. *Cell*. 126:435–439. doi:10.1016/j.cell.2006.07.019

Shibata, Y., C. Voss, J.M. Rist, J. Hu, T.A. Rapoport, W.A. Prinz, and G.K. Voeltz. 2008. The reticulon and DP1/Yop1p proteins form immobile oligomers in the tubular endoplasmic reticulum. *J. Biol. Chem.* 283:18892–18904. doi:10.1074/jbc.M800986200

Shibata, Y., T. Shemesh, W.A. Prinz, A.F. Palazzo, M.M. Kozlov, and T.A. Rapoport. 2010. Mechanisms determining the morphology of the peripheral ER. *Cell*. 143:774–788. doi:10.1016/j.cell.2010.11.007

Sparkes, I., N. Tolley, I. Aller, J. Svozil, A. Osterrieder, S. Botchway, C. Mueller, L. Frigerio, and C. Hawes. 2010. Five Arabidopsis reticulon isoforms share endoplasmic reticulum location, topology, and membrane-shaping properties. *Plant Cell*. 22:1333–1343. doi:10.1105/tpc.110.074385

Staehelin, L.A. 1997. The plant ER: a dynamic organelle composed of a large number of discrete functional domains. *Plant J.* 11:1151–1165. doi:10.1046/j.1365-313X.1997.11061151.x

Terasaki, M., L.B. Chen, and K. Fujiwara. 1986. Microtubules and the endoplasmic reticulum are highly interdependent structures. *J. Cell Biol.* 103:1557–1568. doi:10.1083/jcb.103.4.1557

Tolley, N., I.A. Sparkes, P.R. Hunter, C.P. Craddock, J. Nuttall, L.M. Roberts, C. Hawes, E. Pedrazzini, and L. Frigerio. 2008. Overexpression of a plant reticulon remodels the lumen of the cortical endoplasmic reticulum but does not perturb protein transport. *Traffic*. 9:94–102. doi:10.1111/j.1600-0854.2007.00670.x

Voeltz, G.K., M.M. Rolls, and T.A. Rapoport. 2002. Structural organization of the endoplasmic reticulum. *EMBO Rep.* 3:944–950. doi:10.1093/embo-reports/kvf202

Voeltz, G.K., W.A. Prinz, Y. Shibata, J.M. Rist, and T.A. Rapoport. 2006. A class of membrane proteins shaping the tubular endoplasmic reticulum. *Cell*. 124:573–586. doi:10.1016/j.cell.2005.11.047

Waterman-Storer, C.M., and E.D. Salmon. 1998. Endoplasmic reticulum membrane tubules are distributed by microtubules in living cells using three distinct mechanisms. *Curr. Biol.* 8:798–806. doi:10.1016/S0960-9822(98)70321-5

Wiederkehr, A., Y. Du, M. Pypaert, S. Ferro-Novick, and P. Novick. 2003. Sec3p is needed for the spatial regulation of secretion and for the inheritance of the cortical endoplasmic reticulum. *Mol. Biol. Cell*. 14:4770–4782. doi:10.1091/mbc.E03-04-0229

Woźniak, M.J., B. Bola, K. Brownhill, Y.-C. Yang, V. Levakova, and V.J. Allan. 2009. Role of kinesin-1 and cytoplasmic dynein in endoplasmic reticulum movement in VERO cells. *J. Cell Sci.* 122:1979–1989. doi:10.1242/jcs.041962

West et al., http://www.jcb.org/cgi/content/full/jcb.201011039/DC1

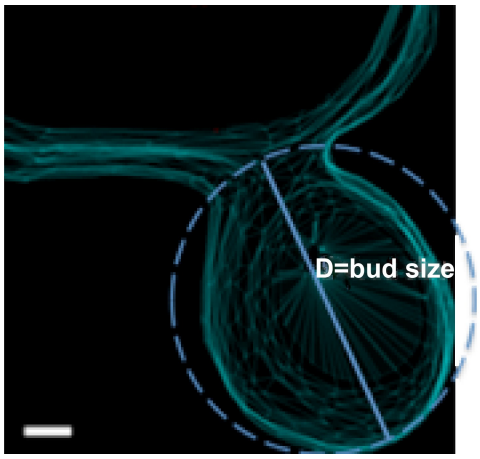

Figure S1. **Diagram to demonstrate how bud sizes were measured.** A sphere is fit from the tip of the bud to the base of the bud. The diameter of the sphere fit (D) equals the bud size. Bar, 200 nm.

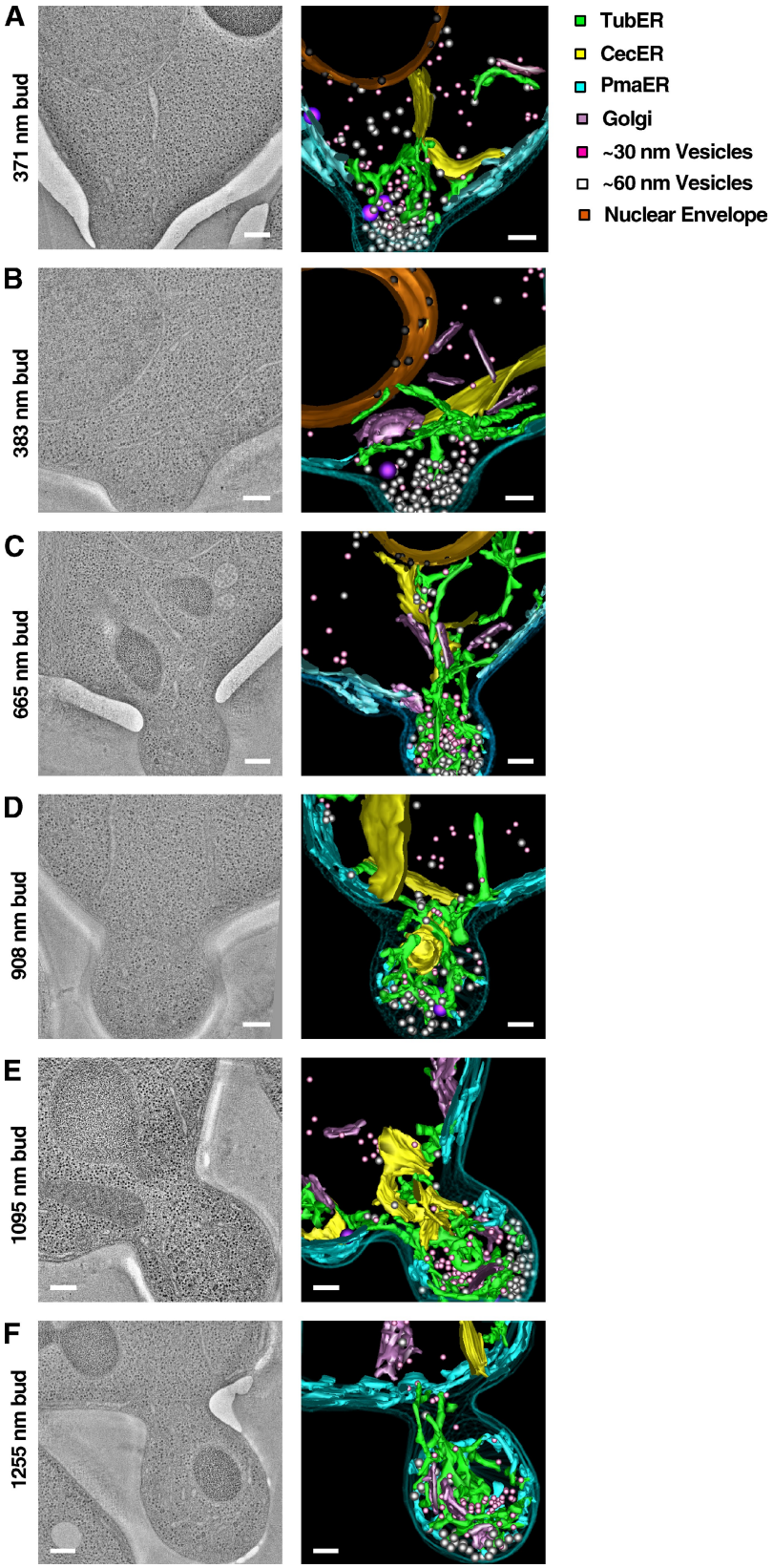

Figure S2. **ER, Golgi, and vesicle distribution during inheritance.** (A–F) 2D tomographs derived from a 200-nm-thick section (left) and 3D models (right) derived from multiple serial sections show ER domain organization, Golgi, the NE, and vesicles in six wt budding yeast cells. The cells are ordered by increasing bud size. Bars, 200 nm.

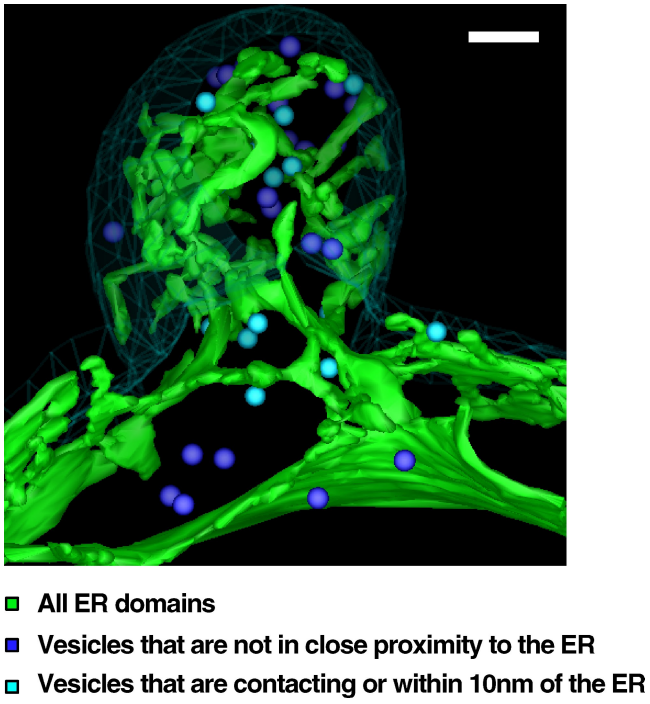

Figure S3. **Vesicles in close proximity or bound to the ER.** Modeled vesicles are shown in light blue that are within 10 nm of the ER membrane. Vesicles in purple are not in close proximity to the ER membrane. Bar, 200 nm.

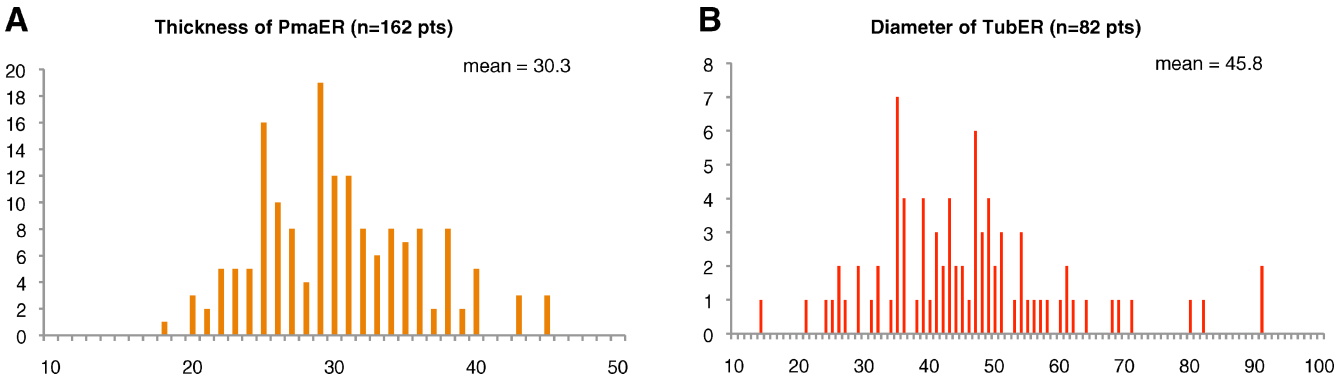

Figure S4. **Histogram of thickness/diameter measurements for mutant ER domains.** (A and B) A histogram showing the range and abundance of the thickness of the pmaER (*n* = 162 width measurements; A) and bud tubER diameters (*n* = 82 diameter measurements; B) in the mutant (mutant = *Δrtn1rtn2yop1*).

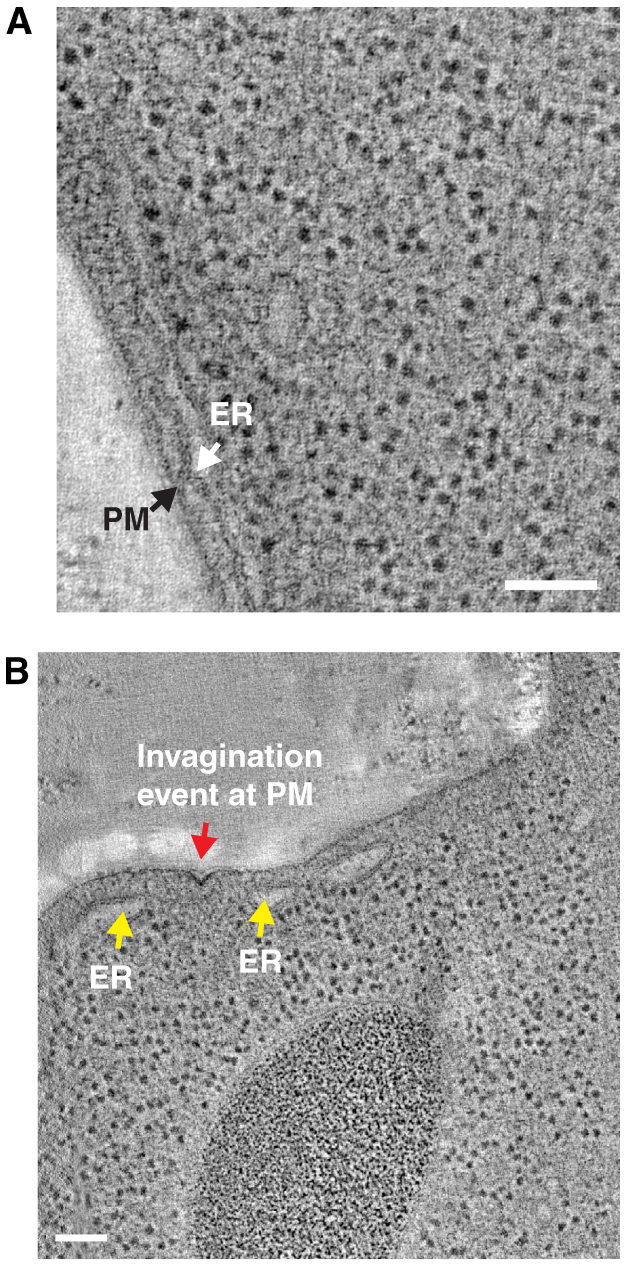

Figure S5. **Images of the PM and pmaER domains.** (A and B) A 2D image derived from a 200-nm-thick section that demonstrates a contact site between the PM and pmaER (white arrow) membrane bilayers (A) and an invagination event at the PM (red arrow) that is occurring at a region away from pmaER–PM contact (B). (B) The pmaER is marked by yellow arrows. Bars, 200 nm.

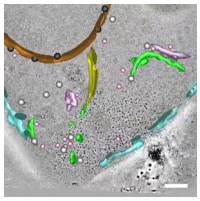

Video 1. **ER domains in 3D in a wt cell with a 371-nm bud (related to Fig. 2).** 3D reconstruction of a wt cell with a 371-nm bud shows all ER domains, Golgi (purple), and vesicles (30 nm is shown in pink, and 60 nm is shown in white). Domains are color coded as in Fig. 2. Bar, 200 nm.

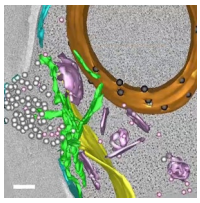

Video 2. **ER domains in 3D in a wt cell with a 383-nm bud (related to Fig. 2).** 3D reconstruction of a wt cell with a 383-nm bud shows all ER domains, Golgi (purple), and vesicles (30 nm is shown in pink, and 60 nm is shown in white). Domains are color coded as in Fig. 2. Bar, 200 nm.

Video 3. **ER domains in 3D in a wt cell with a 665-nm bud (related to Fig. 2).** 3D reconstruction of a wt cell with a 665-nm bud shows all ER domains, Golgi (purple), and vesicles (30 nm is shown in pink, and 60 nm is shown in white). Domains color coded as in Fig. 2. Bar, 200 nm.

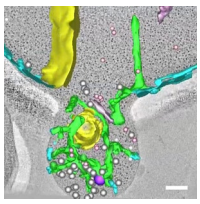

Video 4. **ER domains in 3D in a wt cell with a 908-nm bud (related to Fig. 2).** 3D reconstruction of a wt cell with a 908-nm bud shows all ER domains, Golgi (purple), and vesicles (30 nm is shown in pink, and 60 nm is shown in white). Domains are color coded as in Fig. 2. Bar, 200 nm.

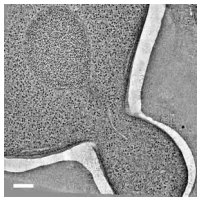

Video 5. **ER domains in 3D in a wt cell with a 1,095-nm bud (related to Fig. 2).** 3D reconstruction of a wt cell with a 1,095-nm bud shows all ER domains, Golgi (purple), and vesicles (30 nm is shown in pink, and 60 nm is shown in white). Domains are color coded as in Fig. 2. Bar, 200 nm.

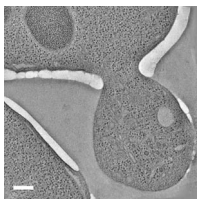

Video 6. **ER domains in 3D in a wt cell with a 1,255-nm bud (related to Fig. 2).** 3D reconstruction of a wt cell with a 1,255-nm bud shows all ER domains, Golgi (purple), and vesicles (30 nm is shown in pink, and 60 nm is shown in white). Domains are color coded as in Fig. 2. Bar, 200 nm.

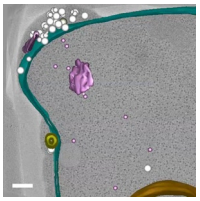

Video 7. **ER domains in 3D in a mutant cell with a 596-nm bud (related to Fig. 4).** 3D reconstruction of mutant cell with a 596-nm bud shows all ER domains, Golgi (purple), and vesicles (30 nm is shown in pink, and 60 nm is shown in white). Domains are color coded as in Fig. 4. Bar, 200 nm.

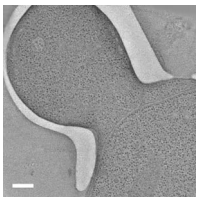

Video 8. **ER domains in 3D in a mutant cell with a 1,253-nm bud (related to Fig. 4).** 3D reconstruction of mutant cell with a 1,253-nm bud shows all ER domains, Golgi (purple), and vesicles (30 nm is shown in pink, and 60 nm is shown in white). Domains are color coded as in Fig. 4. Bar, 200 nm.